



Contents lists available at ScienceDirect

## Journal of Environmental Management

journal homepage: [www.elsevier.com/locate/jenvman](http://www.elsevier.com/locate/jenvman)

# Automatic identification of agricultural terraces through object-oriented analysis of very high resolution DSMs and multispectral imagery obtained from an unmanned aerial vehicle



R.A. Diaz-Varela <sup>a,b,\*</sup>, P.J. Zarco-Tejada <sup>a,c</sup>, V. Angileri <sup>a</sup>, P. Loudjani <sup>a</sup>

<sup>a</sup> Monitoring Agricultural Resources Unit, Institute for Environment and Sustainability, European Commission Joint Research Centre, Via E. Fermi 2749, 21027 Ispra, VA, Italy

<sup>b</sup> Department of Botany, GI-1934-TB, IBADER, University of Santiago de Compostela, Escola Politécnica Superior, Campus Universitario s/n, E-27002 Lugo, Spain

<sup>c</sup> Instituto de Agricultura Sostenible (IAS), Consejo Superior de Investigaciones Científicas (CSIC), Córdoba, Spain

## ARTICLE INFO

### Article history:

Received 17 July 2013

Received in revised form

28 November 2013

Accepted 5 January 2014

Available online 29 January 2014

### Keywords:

Common agricultural policy

Agricultural terraces

Very high resolution imagery

Digital surface model

Unmanned aerial vehicles

Object-oriented analysis

## ABSTRACT

Agricultural terraces are features that provide a number of ecosystem services. As a result, their maintenance is supported by measures established by the European Common Agricultural Policy (CAP). In the framework of CAP implementation and monitoring, there is a current and future need for the development of robust, repeatable and cost-effective methodologies for the automatic identification and monitoring of these features at farm scale. This is a complex task, particularly when terraces are associated to complex vegetation cover patterns, as happens with permanent crops (e.g. olive trees). In this study we present a novel methodology for automatic and cost-efficient identification of terraces using only imagery from commercial off-the-shelf (COTS) cameras on board unmanned aerial vehicles (UAVs). Using state-of-the-art computer vision techniques, we generated orthoimagery and digital surface models (DSMs) at 11 cm spatial resolution with low user intervention. In a second stage, these data were used to identify terraces using a multi-scale object-oriented classification method. Results show the potential of this method even in highly complex agricultural areas, both regarding DSM reconstruction and image classification. The UAV-derived DSM had a root mean square error (RMSE) lower than 0.5 m when the height of the terraces was assessed against field GPS data. The subsequent automated terrace classification yielded an overall accuracy of 90% based exclusively on spectral and elevation data derived from the UAV imagery.

© 2014 Elsevier Ltd. All rights reserved.

## 1. Introduction

In recent years, the European Common Agricultural Policy (CAP) has been integrating environmental concerns and moving towards the enhancement of agricultural services provided to society as well as innovation and support of rural sustainable development (European Commission, 2012a). In this framework, since 2005 farmers have had to comply with common rules and standards regarding the environment as well as public, animal and plant health and animal welfare. Such standards are known as 'cross-compliance' (Council Regulation EC No 73/2009). In addition,

further measures are under discussion regarding the 'greening' of direct payments (COM(2001) 625).

As a component of cross-compliance, in order to obtain full 'single farm payments,' farmers are required to keep agricultural land in Good Agricultural and Environmental Condition (GAEC) by respecting a number of minimum requirements regarding the prevention of soil erosion, the conservation of soil organic matter and structure and the maintenance of habitats and landscape features. Furthermore, one of the measures proposed for the 'greening' of payments establishes that farmers shall ensure that a certain amount of their agricultural land is kept as 'Ecological Focus Areas' (EFAs), which refers to a set of elements that deliver habitat and water protection.

Agricultural terraces are among the elements taken into account in both the GAEC and the EFA proposals. In fact, agricultural terraces provide several ecosystem services when they are properly built and managed. Most of these services are related to ground

\* Corresponding author. Department of Botany, GI-1934-TB, IBADER, University of Santiago de Compostela, Escola Politécnica Superior, Campus Universitario s/n, E-27002 Lugo, Spain.

E-mail addresses: [ramondiaz06@gmail.com](mailto:ramondiaz06@gmail.com), [ramon.diaz@usc.es](mailto:ramon.diaz@usc.es) (R.A. Diaz-Varela).

surface leveling and stabilization of slopes by enhancing water infiltration and reducing erosion risks (McNeill, 1992; Rey Benayas et al., 2007). However, agricultural terraces also increase landscape diversity and can function as habitat providers and biodiversity corridors (Pereira et al., 2006). By contrast, when such terraces are poorly designed or managed or degraded, they can collapse and aggravate erosion processes (Martínez-Casasnovas et al., 2010; Dunjó et al., 2003).

European national authorities manage subsidies granted to farmers and verify whether legal requirements are met through the Integrated Administration and Control System (IACS). In the framework of GAEC, they must ensure that farmers maintain terraces in good condition and do not remove them. This requires identifying terraces and monitoring their presence and conservation status over the years. In the context of the proposed EFAs, land occupied by terraces must also be quantified to calculate the EFA at farm level.

Therefore, in the framework of CAP implementation and monitoring, there is a current and future need for the development of robust, repeatable and cost-effective methodologies for the automatic identification and monitoring of features that provide ecosystem services at farm scale. So far, most efforts have focused on the automatic identification of linear or point features such as tree lines, hedges or field margins from very high resolution imagery using spectral, textural and shape features (Sheeren et al., 2009; Aksoy et al., 2010) or including additional information from digital terrain and surface models (Tansey et al., 2009). In this regard, use of high-resolution 3D information and particularly of very high resolution digital surface models (DSMs, i.e. models that represent the earth's surface and include any objects on it) has shown potential for the identification and monitoring of linear landscape features (Bailly and Levvasseur, 2012).

Few studies have specifically been aimed at identifying and monitoring agricultural terraces at a detailed scale (see some examples in Karydas et al., 2005; or Martínez-Casasnovas et al., 2010). By contrast, examples of terrace identification from large-scale remote sensing imagery or digital elevation models are far more frequent in the context of geomorphology studies (see, e.g. Demoulin et al., 2007; or Clarke et al., 2010). In the particular case of agricultural terrace identification, most studies are based on the visual interpretation of orthoimages (Faulkner et al., 2003; Martínez-Casasnovas et al., 2010; Agnoletti et al., 2011) while automated approaches are much scarcer (Karydas et al., 2005; Li et al., 2012; Bailly and Levvasseur, 2012).

Use of unmanned aerial vehicles (UAVs) for civil applications such as high-resolution image acquisition has emerged as an attractive and flexible option for the monitoring of various aspects of agriculture and the environment (see, e.g. Amorós López et al., 2011; Laliberte et al., 2010; Reid et al., 2011; Wallace et al., 2012; Zaman et al., 2011). Progress made in the miniaturization and cost-reduction of inertial sensors, GPS devices and embedded computers has enhanced the possibilities of remote sensing using a new generation of commercial off-the-shelf (COTS) instruments (Berni et al., 2009a) with a wide range of potential applications. Recent studies have demonstrated the feasibility of applying quantitative remote sensing methods to vegetation monitoring using miniature thermal cameras (Berni et al., 2009a, 2009b; González-Dugo et al., 2012), narrow-band multispectral imagery (Zarco-Tejada et al., 2009; Suárez et al., 2010; Guillén-Climent et al., 2012) and micro-hyperspectral imagery (Zarco-Tejada et al., 2012, 2013a; 2013b).

The generation of accurate orthoimages (2D) and DSMs (3D) usually relies on rigorous photogrammetric methods or—in the case of 3D images—on laser scanners such as LIDAR. Both options require expensive and precise technology and/or highly qualified users. An alternative to traditional photogrammetry or active sensor technologies is to take advantage of the information

contained in large sets of multi-angle images obtained by consumer-grade cameras and referenced by low-cost miniature GPS receivers and inertial sensors operating on UAV platforms. In fact, state-of-the-art computer vision techniques enable the generation of reliable 2D and 3D imagery from these collections using 3D photo-reconstruction algorithms based on structure-from-motion and multiview-stereo analysis algorithms (James and Robson, 2012; Küng et al., 2011).

The classification of spatial clusters of pixels generated through image segmentation has become a popular alternative to classic single-pixel-oriented classifications in the field of remote sensing. These spatial clusters, often referred to as 'image objects' or 'image segments,' are usually defined as discrete regions of images that are internally coherent and different from their surroundings (Castilla and Hay, 2008). Object-oriented analysis has shown important advantages over traditional pixel-oriented analysis, particularly in very high resolution imagery classification (Blaschke, 2010; Drägut et al., 2010). In fact, object-oriented analysis of meaningful spatial entities is a way of including image texture or context information while allowing an easy integration of several scales of analysis. This strategy successfully takes into account the multi-scale perception of landscape and the heterogeneity of its components, thus facilitating its classification (Burnett and Blaschke, 2003).

Considering the above-mentioned points, the aim of the present study was to generate and validate cost-efficient methodologies for the identification of agricultural terraces using very high resolution imagery. Our specific objectives were i) to evaluate the potential of low-cost non-metric cameras on board a UAV for DSM relief reconstruction in areas with agricultural terraces; and ii) to develop and validate a methodology for object-oriented automatic identification of agricultural terraces using multispectral information and DSMs generated from the above-mentioned imagery.

## 2. Material and methods

### 2.1. Overview of the analyses

The workflow of this study can be summarized into four main stages: i) acquisition of the imagery, ii) pre-processing of the UAV imagery to generate the green-red-near infrared orthomosaic and the digital surface model along with derived products, iii) classification of the imagery in order to create a binary Terrace/No terrace map and iv) ground truth data collection and validation of both the DSM and the classification accuracy (Fig. 1).

### 2.2. Study area and datasets

The analyses were conducted in a test area of about 120 ha located in the province of Cordoba (southern Spain) covering an agricultural setting mainly occupied by olive orchards. Olive trees are cultivated either in rows or in patterns both on terraced and non-terraced land (Fig. 2). The elevation of the study site ranges from 370 to 550 m above sea level (ASL) with predominant east and south slope aspects. Relief can be considered rough from an agronomic point of view, with slope values ranging from flat to a maximum of 37°, a mean slope of 12° and a standard deviation of 4.2°.

The airborne campaign was conducted in 2012 with an unmanned aerial vehicle (UAV) operated by the Laboratory for Research Methods in Quantitative Remote Sensing (QuantaLab, IAS-CSIC, Spain). The UAV carried a CIR Panasonic Lumix DMC-GF1 camera (Berni et al., 2009a; Zarco-Tejada et al., 2008, 2012, 2013a) with a 4000x3000 pixel detector that captured images at  $f/3.2$  and  $1/2500$  s with an angular FOV of  $47.6^\circ \times 36.3^\circ$  and provided 11 cm pixel resolution at an altitude of 500 m above ground level (AGL). The ground footprint size for an individual image was

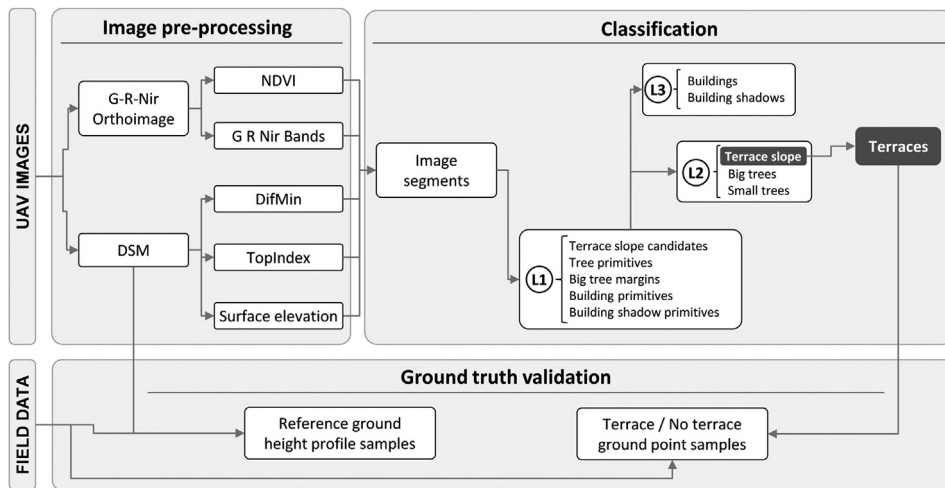


**Fig. 1.** Analysis flowchart. The image pre-processing block shows the UAV data processing used to generate the inputs for classification. The classes generated for each classification level (L1, L2 and L3) are specified in the classification block. The ground truth validation illustrates the accuracy assessments of the DSM reconstruction and terrace classification respectively.

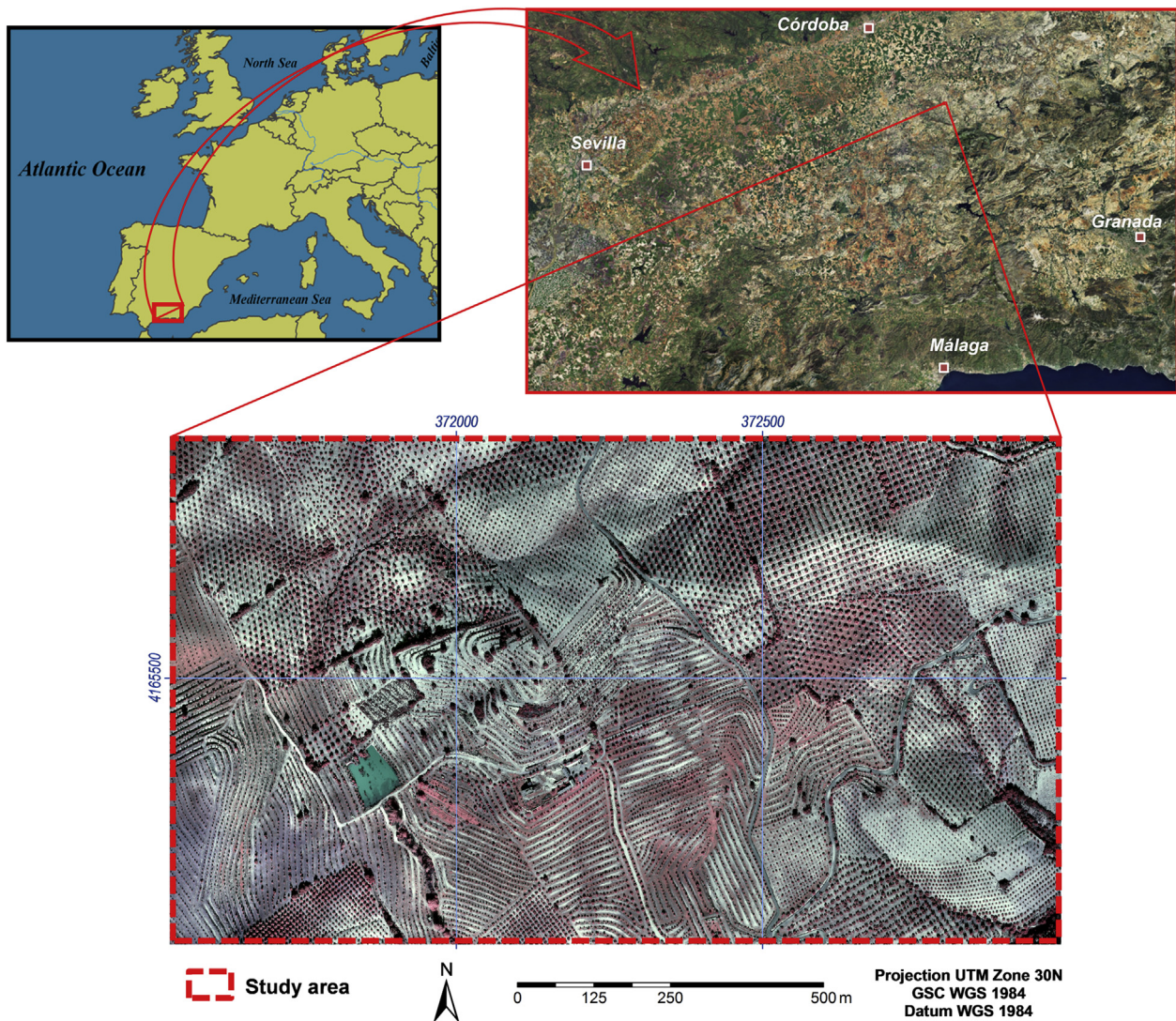


**Fig. 2.** Study area (Base map source: ESRI Inc.; Bing maps).

approximately  $325 \times 430$  m. The camera was modified from RGB to CIR by removing the internal NIR filter. The UAV platform operated was a 2-m wingspan fixed-wing platform with up to 1-hour endurance at 5.8 kg take-off weight (TOW) and 63 km/h ground speed (mX-SIGHT, UAV Services and Systems, Germany). It was controlled by an autopilot for autonomous flying (AP04, UAV Navigation, Madrid, Spain) and followed a flight plan using waypoints to acquire imagery from the study area. The autopilot had a dual CPU controlling an integrated Altitude Heading Reference System (AHRS) based on a L1 GPS board, 3-axis accelerometers, gyros and a 3-axis magnetometer (Berni et al., 2009a). The ground control station and the UAV were radio linked, transmitting position, altitude and status data at 20 Hz frequency. This tunneling transmission link was used for the operation of the cameras from the ground station deployed near the study sites.

### 2.3. Image processing

The 432 airborne images acquired during the flight were used to generate the orthomosaic and the DSM reconstruction using Pix4UAV software (Ecublens, Switzerland). In this image processing stage, the input was the imagery and the altitude data acquired during the flight, using synchronized GPS position and roll, pitch and yaw for each single image. The point cloud densification parameter was set to high and the grid sampling distance in the DEM point cloud was set to 100 cm. The orthomosaic was obtained in 5000x5000 pixel tiles with a blending factor of 0.5. The camera parameters were optimized internally in the initial stage. An orthomosaic and a DSM, both with a spatial resolution of 0.11 m, were obtained in this process and used in the subsequent classification stage. The Normalized Difference Vegetation Index (NDVI, Equation (1)) was calculated from the raw red and NIR band radiance values of the generated orthomosaic as a measure of the vigor of the vegetation cover.

$$\text{NDVI} = (\text{NIR} - R) / (\text{NIR} + R) \quad (1)$$

where

$$\begin{aligned} R &= \text{pixel value of the red image band} \\ \text{NIR} &= \text{pixel value of the near infrared image band} \end{aligned}$$

Several terrain parameters were also derived from the computed DSM, namely the difference from the minimum value (DifMin) in a search circle of 2 m around the target pixel (Equation (2)) and a topographic position index (TopIndex) based on the concept developed by McNab (1989) of the Terrain Shape Index using a circular neighborhood of 5 m (Equation (3)). These parameters were preferred to the gradient slope because the latter is more prone to fine-scale artifacts. Gradient slope is also more sensitive to the presence of inclination in the plane of the terrace leveled surface. These indices were used to identify the various terrain irregularities associated with terrace slopes, trees and buildings in the classification procedure (see Section 2.4).

$$\text{DifMin} = h_i / h_{\min} \quad (2)$$

$$\text{TopIndex} = h_i / h_{\text{ave}} \quad (3)$$

where

$$\begin{aligned} h_i &= \text{DSM value for the target pixel} \\ h_{\min} &= \text{Minimum DSM value for a given neighborhood around the target pixel} \\ h_{\text{ave}} &= \text{Average DSM value for a given neighborhood around the target pixel} \end{aligned}$$

### 2.4. Terrace classification

In order to identify the terraces, we conducted an object-oriented classification using eCognition Developer 8<sup>®</sup> software (© TRIMBLE Germany GmbH), where the features to be classified are not single pixels but spatial pixel clusters defined through an aggregation algorithm known as 'multiresolution segmentation' (Baatz et al., 2004; Benz et al., 2004). The algorithm is based on a bottom-up iterative spatial aggregation of objects with low spatial entity (i.e. individual pixels) so as to minimize heterogeneity and is weighted by the final segment size. The segmentation algorithm integrates texture criteria by considering size uniformity, pixel values and local contrast for the elements contained in a given segment. In practice, the segmentation process is controlled by the user by setting scale and homogeneity parameters. Scale parameters control the final size of the segments while homogeneity parameters control the internal heterogeneity of the segments, both in terms of spectral (or color) and shape characteristics (see Burnett and Blaschke, 2003 for a more thorough discussion on the topic). We used this classification approach due to its versatility to integrate context information and perform a multi-scale analysis, given that it enables the identification of topological relationships between image objects at a given scale level and also across spatial scales at different hierarchical levels.

We started from the assumption that terraces could be delineated by identifying their slopes, defined as long linear elements with an abrupt change in elevation. The classification process was conducted in two stages: segmentation of the image into meaningful objects (i.e. spatial aggregation of pixels) in the context of the classification targets and classification of these elements (i.e. assigning objects to the semantic classes Terrace/No terrace).

In the first stage, we used a simple level of segmentation, adjusting the parameters so that image objects would fit with real-world target elements (basically groups of pixels corresponding to sections of terrace slopes and also buildings and small trees). We located these elements in the image by visual inspection and subsequently verified them in the field. We used this manual procedure instead of other more automated approaches (see, e.g. Drăgut et al., 2010) as we targeted very specific elements that represent a small share of the image, that is, the 'building blocks' of the final classes to be identified (Hofman et al., 2011), rather than the scale- or scales- representing the most prominent levels of organization within the whole image.

Segmentation parameter values were adjusted iteratively using a trial-error procedure, comparing segment edges against known reference areas. A certain degree of over-segmentation was allowed in order to enable a good delineation of the elements in the image. The data layers Surface elevation, DifMin and NDVI were weighted by one while the Red, Green and NIR image bands and the TopIndex data layer were weighted by 0.5. The shape parameter (i.e. shape vs. spectral importance, ranging from 0 to 1) was set to 0.2 while the compactness parameter (i.e. compactness vs. smoothness of segments, ranging from 0 to 1) was set to 0.5.

In the second stage, a classification model was constructed based on conceptual rules with a three-level hierarchical structure using a bottom-up approach. In a first step of the classification, buildings and their shadows were identified and masked out for the subsequent classification steps. Hence, building primitives were identified in the basic level (referred to as L1 in the block classification of Fig. 1) as objects with low NDVI and high TopIndex values. Next, adjacent building primitives were merged at a new higher hierarchical level (referred to as L3 in the block classification of Fig. 1), where composite objects larger than a certain area and significantly higher than their surroundings (i.e. with high border contrast in the DSM) were finally assigned to the Building class.

Shadows of building primitives were identified as L1 objects with low NIR values and subsequently merged in L3 composite building shadow candidates. After that, they were classified as building shadows if they shared more than 20% of their border with elements of the Building class.

In a second step, slope anomalies corresponding to abrupt changes in elevation were calculated from the DSM and used for the identification of terrace slope candidates. These slope anomalies were defined as objects with relatively high DifMin values as a feature potentially related to the occurrence of terrace slopes. From this point, the discrimination of large trees, large tree margins and small trees was addressed. A class of tree candidates was defined at L1 as slope anomalies with high NDVI and TopIndex values. L1 tree candidates were then merged at a higher hierarchical level (referred to as L2 in the block classification of Fig. 1) and reclassified as large or small trees using the L2 object area and DifMin as discrimination criteria (i.e. tree crown size and height). Slope anomalies surrounding large trees were finally classified as large tree margins.

The remaining objects of the Slope anomaly class were merged with the Small trees class at L2. These two classes were aggregated because of the characteristics of the study area, where terraces are mainly planted with small olive trees. A morphological opening filter was then applied to the resulting L2 objects in order to smooth their contour and avoid artifacts in these elements. At this point, a collection of terrain anomalies semantically likely to correspond to the slope of terraces (terrace candidates) was identified. Yet, in some cases these elements could still be confused with the transition between tree crowns and the ground surface as recorded by the DSM. We therefore introduced a new rule at L2 level in order to retain only terraces with high length and length/width values. In a final classification refinement, L2 terrace candidates with a high relative share of small tree sub-objects were excluded from the final terrace class in order to avoid confusions between rows of trees with crown closure or with vegetated terraces.

The final extent of terraces was calculated by applying a buffer of 6 m around the objects on the terrace slope, resulting in compact

polygons covering the targeted terrace area. This buffer width was chosen as a slightly higher value than 1/2, the standard width of the terraces for this particular area study area. Polygons with a surface of less than 1 ha were masked out of the Terrace class as they were likely to correspond to roadside slopes, tree clumps or other features instead of terraced land.

## 2.5. Validation

The validation was conducted at two levels: i) a first level to assess the actual accuracy of the UAV-derived DSM in identifying the morphology of terraces and ii) a second level to assess the accuracy of the categorical binary map of the Terrace/No terrace classification method.

In the first case, a series of 14 transects (see Fig. 3) with lengths from 100 to 200 m was established as independent reference data; absolute ground elevation was recorded at horizontal intervals ca. 1 m and characteristic points were covered along the terrace profile (i.e. at least at the beginning and end of slopes and flat surfaces). Measures were taken with a differential TRIMBLE R6 GPS receiver in RTK (Real-Time Kinematic) mode with an XY precision of 8 mm and a Z precision of 15 mm. The transects were designed to cover the possible variations in slope, aspect and degree of terrace definition across the area. The DSM was co-registered to the transect reference system and the modeled DSM elevation was extracted for all the transect points. As the DSM used relative XYZ coordinates and our interest was to check relative ground differences between real ground elevation and the DSM so as to identify terraces, elevation differences between sequential pairs of points along the transects were compared. Therefore, the Root Mean Square Error (RMSE) for each transect was computed taking into account the residuals (DSM against ground truth) of the height differences between pairs of points. The squared Pearson correlation coefficient between the DSM and ground truth elevation for each transect was also calculated as an alternative measure of DSM accuracy.

Terrace classification accuracy was computed from a reference set of independent validation points distributed randomly in the

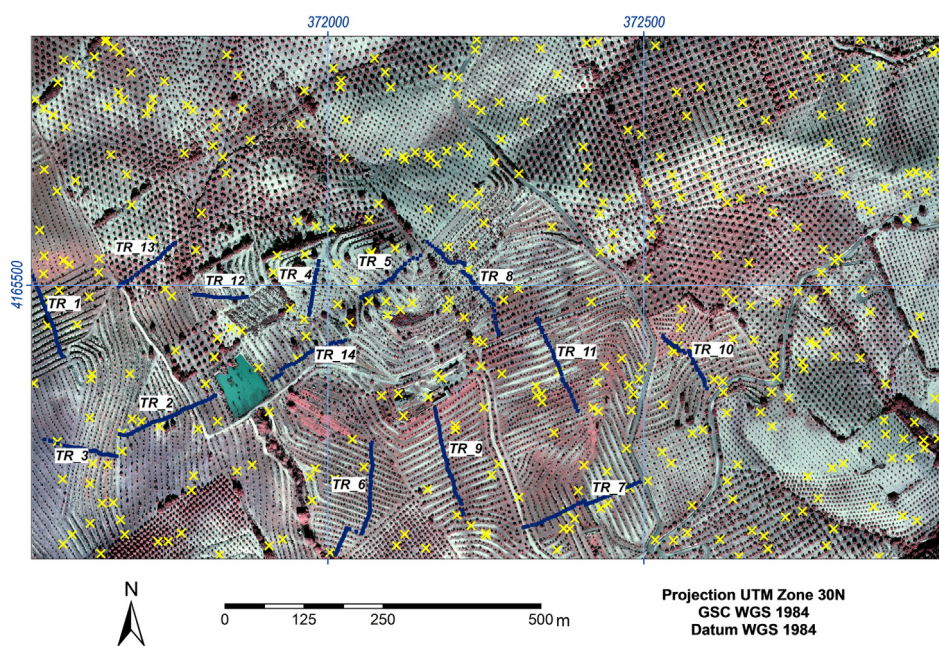


**Fig. 3.** DSM validation transects (in blue) numbered from TR 1 to TR 14 and terrace classification validation points (yellow crosses) in the study area. (For interpretation of the references to color in this figure legend, the reader is referred to the web version of this article.)

study area. We used a classic approach using random validation points as the objective was to determine the accuracy of the final classification (ensured by the use of the appropriate accuracy indices and a probabilistic sampling with sufficient number of samples) rather than assessing the performance of the segmentation procedure in terms of the delineation of geometrical elements (i.e. segments). Points were located in the field using the same GPS device used in the transect surveying and the presence/absence of terraces was ascertained by field inspection. Sample size was calculated based on the expression applicable to multinomial tests and variables (Tortora, 1978) for a two-class classification scheme, a 0.1 probability of Type I error and 95% precision in the results. The highest class frequency was set to 50% as the worst case scenario of class frequency. The minimum sample size was 384 and a final sampling size of 400 verification points was adopted in order to exceed this minimum number. Classification values were retrieved for these point locations by field inspection and compared with reference data by cross-tabulation in an error matrix. Several accuracy statistics were then computed, namely overall classification accuracy and Cohen's Kappa coefficient, along with omission/commission errors and the conditional Kappa coefficient at class level (Bishop et al., 1975; Congalton, 1991).

### 3. Results

#### 3.1. Orthorectification and digital surface model

For the process of orthorectification, mosaicking and DSM interpolation, 430 out of the 432 original images were used. The resulting mosaic covered an area of 192.5 ha, of which a core area of 120 ha was extracted for the analyses. The mean GSD (i.e. size of a pixel on the ground) of the original images was computed at 10.97 cm. The bundle block adjustment process took into account 257 040 key points, using a total of 85 400 points for the 3D bundle block adjustment. Mean re-projection error was estimated at

0.9163 pixels (ca. 10.05 cm). A visual example of the general appearance of the DSM along with detailed views of areas with and without terraces is shown in Fig. 4.

Fig. 5 shows the along-slope profiles of two areas compared: one corresponds to terraced land and the other corresponds to non-terraced land. Despite the differences between the two transects in overall height ranges and the existence of some noise due to the presence of tree protrusions in the DSM, differences in the underlying ground surface between land with (A) and without terraces (B) are clearly seen.

Results of the elevation difference accuracy assessment showed a high agreement between the DSM and the reference data (Fig. 6). In fact, most of the transects evaluated (10 out of 14) had an RMSE lower than 0.60 m, while the average RMSE for the 14 transects was 0.49 m. Likewise, the squared Pearson correlation between model and reference data ( $R^2$ ) reached values equal to or higher than 0.99 for all the transects evaluated.

#### 3.2. Terrace classification

An overview of the terrace classification results is presented in Fig. 7. According to the classification results, 27.75% of the area was labeled as terraces (33.31 out of 120 ha). Terrace areas were clustered in the south part of the study area, where some potential omission errors were apparent as small gaps in terrace plots. The rest of the area was assigned to the No terrace class. The commission errors of the Terrace class were far more uncommon in this sector.

The confusion matrix and per-class classification accuracy statistics are summarized in Table 1. Overall accuracy and Kappa statistics reached 90.25% and 0.77 respectively. According to the qualitative scale developed by Landis and Koch (1977) for the Kappa coefficient, both the overall classification and the No terrace class reached a substantial agreement with the reference data (Kappa values in the 0.61–0.80 interval) while the Terrace class

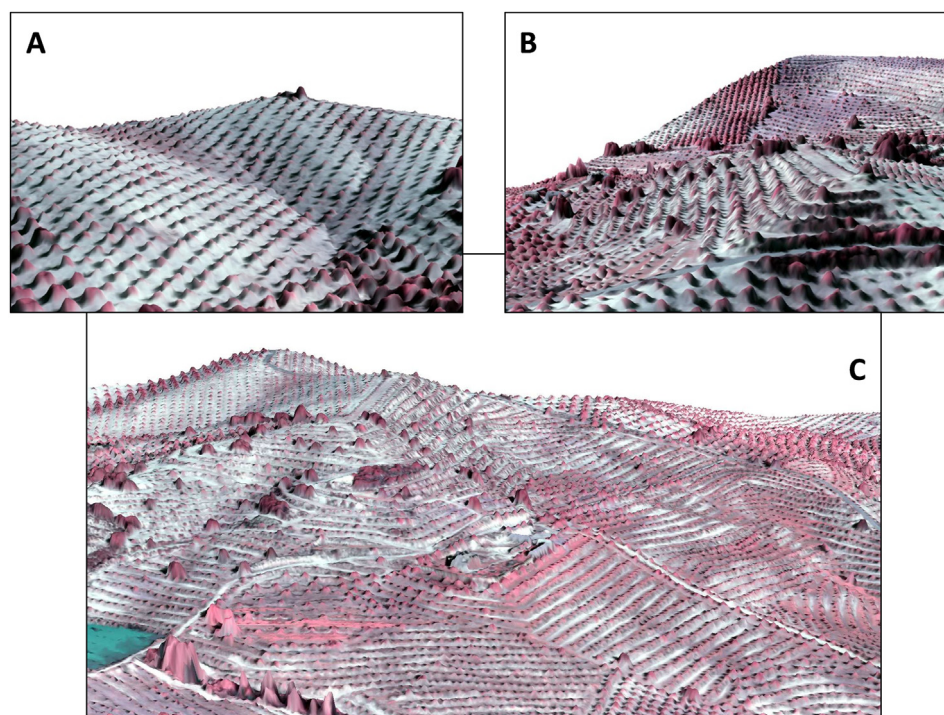


Fig. 4. 3D Block detailed view of two areas without (A) and with (B) terraces and general overview (C) of the DSM and othomosaic generated in the study. The 3D block was obtained with ENVI 5.0 software (© 2012 Exelis Visual Information Solutions Inc.).

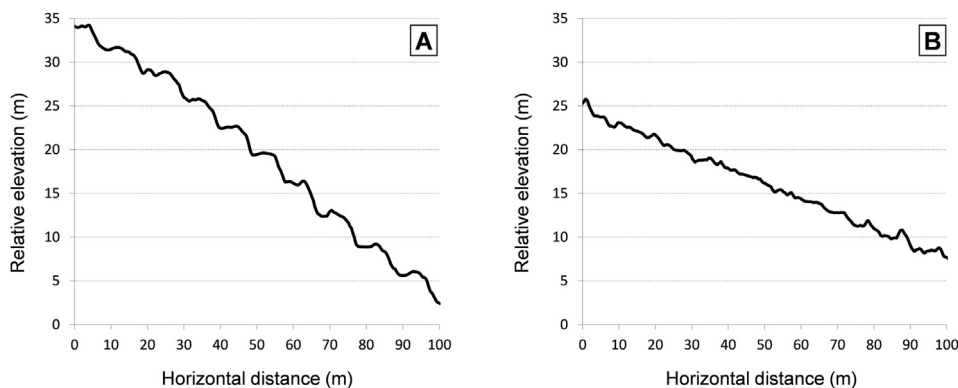


Fig. 5. Surface profiles extracted from the DSM image. A: Terraced area; B: Non-terraced area. X axis: distance in m; Y axis: relative elevation in m.

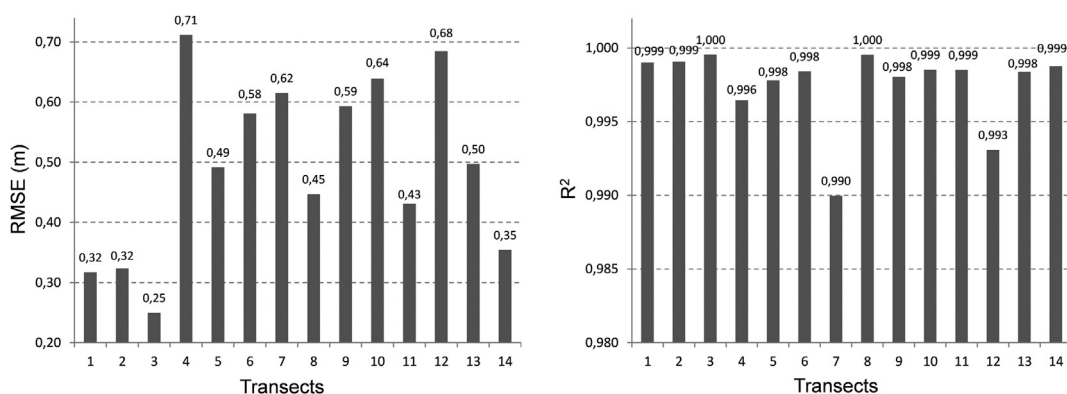


Fig. 6. RMSE (left) and squared Pearson correlations (right) between the DSM and reference values for the 14 transects measured.

reached an almost perfect agreement with the reference data (Kappa values higher than 0.81). According to the other quantitative scale widely used in remote sensing (Fleiss, 1981), the overall Kappa and the Terrace class conditional Kappa values can be

considered to show excellent agreement with the reference data (i.e. Kappa values higher than 0.75) while the No terrace class conditional Kappa exhibited a good agreement with the reference data (i.e. Kappa values in the 0.40–0.75 interval).

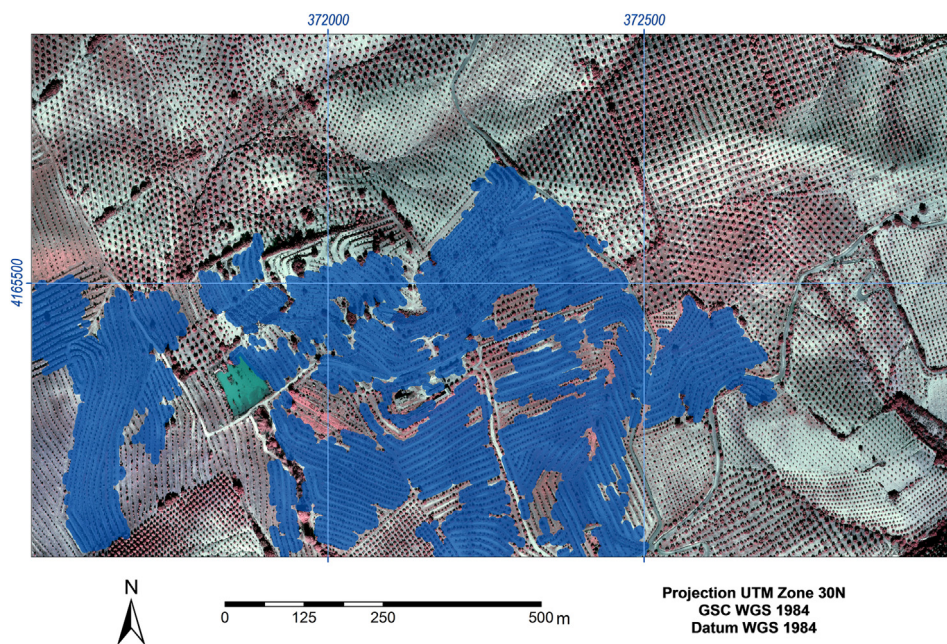


Fig. 7. Overview of the terrace classification output. Blue shading represents areas classified as terraces. (For interpretation of the references to color in this figure legend, the reader is referred to the web version of this article.)

**Table 1**  
Error matrix and per-class accuracy statistics of the terrace classification. Reference: reference (ground truth) frequencies (in columns); Classification: per-class classification frequencies (in rows); Class. Totals: per-class classification totals; Ref. totals: per-class reference totals; Prod. Ac.: Producers' accuracy; User Ac.: Users' accuracy; Omi. Er.: Omission error; Com. Er.: Commission error; Cond. Kappa: Per-class conditional Kappa.

Classification	Reference		Class. totals	Prod. Ac.	User. Ac.	Omi. Er.	Com. Er.	Cond. Kappa
	No terraces	Terraces						
No terraces	259	34	293	98,11	88,40	1,89	11,60	0,66
Terraces	5	102	107	75,00	95,33	25,00	4,67	0,93
Ref. totals	264	136	400					

#### 4. Discussion

Automatic identification of agricultural terraces using remote sensing is not a trivial issue, particularly in the case of complex landscape patterns and diverse vegetation cover. The scale of the target elements hampers the applicability of methods and datasets frequently used in geomorphology and landform analysis (see, e.g. Tagil and Jenness, 2008.). In addition, the use of spectral data only can be insufficient for reaching the accuracy standards required for agricultural policy implementation at farm level. The use of high-resolution imagery along with elevation data in the classification process is a promising approach for the identification of small-scale landscape features in general (Hou and Walz, 2013) and agricultural terraces in particular (Bailly and Levvasseur, 2012). In this paper, we explored the possibilities of low-cost high-resolution UAV imagery for solving this complex problem. In the first stage of the research, we obtained accurate results for surface relief reconstruction, a key issue for further implementation of the automatic classification procedure. More specifically, we obtained an average disagreement (i.e. RMSE after horizontal bias correction) of less than 50 cm between the DSM and the GPS ground survey. It should be noted that these results were obtained without Ground Control Point surveying, that is, using a fully automatic method in the aerial photo reconstruction and therefore optimizing the time devoted to data acquisition and processing and overall cost effectiveness. The accuracy achieved was therefore comparable to that of very high resolution DSMs obtained using much more expensive technologies, such as LIDAR with point density higher than one point per square meter (Artuso et al., 2003). Taking into account the roughness of the ground and other possible artifacts, the error can be considered low for the following reasons: first, the target features (i.e. terrace slopes) typically range between 1.5 and 2.5 m in height in the area, and second, ground surface irregularities smaller than 0.5 m can hardly be considered as terraces.

The potential of stereo imagery for the control of CAP measures using remote sensing has been tested from different points of view (Åstrand et al., 2012). In general, one-dimension orthoimagery derived from high-resolution satellite stereo pairs (e.g. WorldView-2, with ground pixel size around 0.5 m) easily meets the standards for CAP monitoring with remote sensing for plot identification (European Commission, 2012b), that is, 2.5 m maximum error in X and Y coordinates, provided that a good quality DEM is used. Digital surface models generated from the same data source also can reach these standards, with Z (elevation) RMSE as low as 2–3 m, provided that state-of-the-art DSM creation software and accurate ground control points are used (Capaldo et al., 2010; Åstrand et al., 2012). In our case study and taking into account the dimensions of the target elements, use of higher-resolution and especially higher-accuracy DSMs might be advisable for the identification and analysis of agricultural terraces. This is particularly true when there is the additional difficulty of heterogeneous vegetation coverage that might distort ground surface relief, as discussed below.

In the second stage of the analysis, we integrated spectral and surface information in order to accurately identify the area of terraces. Spatial context and multiple scale analyses were performed to maximize the classification performance, taking into account previous experiences in landscape feature identification (Tansey et al., 2009; Aksoy et al., 2010) and terrain morphology analysis (Drăguț and Blaschke, 2006). In several examples of DSM analysis (e.g. urban or forest areas), the normalized digital surface model (NDSM, as the difference between DSM and DEM) is often calculated prior to the classification in order to identify off-terrain elements such as trees or buildings (Waser et al., 2008). This can be easily done when an adequate resolution and co-registered DEM is available by using simple algebraic difference or alternatively by using algorithms such as different types of morphological filtering (Krauß et al., 2011). In our case, no very high resolution DEMs were available. Thus, for the sake of simplicity and in order to maximize control of the process and take full advantage of the multiscale object-oriented analysis, we chose to include the raw DSM and several derived topographic features in the classification along with spectral information, all taken in a single data acquisition.

The classification was conducted as a multiscale iterative process, where large size elements corresponding to surface height anomalies (i.e. buildings, large trees and tree clumps and lines) were first masked out to identify terraces and trees growing on their leveled surfaces. A key stage in this classification was the identification of closed-canopy lines of trees on non-terraced slopes and their discrimination against real terraces with tree rows along their flat surfaces. To overcome this problem, we used multi-scale classification rules based on spatial context and object morphological operators.

The classification results confirmed the potential of low-cost imagery for the accurate identification and further monitoring of terraces in the framework of CAP implementation, exceeding the commonly recommended targets in remote sensing land cover classification of 85% minimum overall accuracy and 75% individual accuracy (Foody, 2002). We obtained an overall accuracy of 90% and a kappa index indicating a substantial agreement between classification and field reference data. From a per-class point of view, both users' and producers' accuracies (complementary to the omission and commission errors respectively) were at or above 75% for all classes.

As regards the implications of classification quality for CAP implementation and monitoring, it is worth highlighting that the omission error for the No terrace class was lower than 2%. Therefore, the 'specificity' of the prediction, that is, the probability that a real absence site was correctly predicted (Fielding and Bell, 1997), was higher than 98%. Commission errors also remained at relatively low values for the Terrace class (less than 5%) and the No terrace class (less than 12%). This means that there were few chances of predicting inclusion in the classes when the element should be excluded. By contrast, omission errors were higher (25%) for the Terrace class. This means that the classification settings were very conservative in terms of reducing the risk of classifying non-terraced land as terraces while maintaining quite high accuracies

for both classes from the final user viewpoint (Congalton and Green, 1999), at the risk of missing some actual terraced land in the classification. As a consequence, it would be unlikely to miss a situation of possible terrace removal when comparing time series of maps generated using this method for the monitoring of terrace persistence. In fact, we were able to accurately predict the true presence of terraces for a specific initial reference date, as we obtained a commission error lower than 5% for the Terrace class (i.e. a positive predictive power higher than 95%). Likewise, it would be very unlikely to miss the No terrace class for a final reference date, as very low omission errors were foreseen using this methodology (i.e. omission errors for the No terrace class were lower than 2%).

The methodology presented in this work can easily be transferred to other terrace identification problems, provided that some key classification parameters are refined and that the dimensions and coverage of the tree crops are smaller than the terrace slopes and flat surfaces respectively. Parameters most in need of refinement are those related to the geometry of the targeted elements (i.e. the width of the leveled surface of terraces or the height difference of the terrace slope) and those related to the structure of the vegetation cover or crops on the terraced area. In addition, although they were not the main targets of the classification, other landscape features classified, such as 'large trees,' could correspond to GAEC and EFA elements. This underlines the potential of this methodology to be extended for the identification of other elements of interest in the CAP framework. Finally, the accuracy of the DSM elevations obtained in this study also opens possibilities for a more detailed characterization of such landscape features, measuring aspects such as size or volume as a proxy for the amount of environment services supplied.

## 5. Conclusions

The implementation of the European Common Agricultural Policy requires the development of cost-effective and flexible methods for the identification and monitoring of features providing ecosystem services, such as agricultural terraces. In this work we proposed and tested a low-cost methodology for the automatic classification of agricultural terraces using high-resolution imagery acquired by non-metric cameras on board a low-cost unmanned aerial vehicle (UAV). The premises of this experiment were i) to minimize the cost of image acquisition in the field and ii) to avoid ancillary datasets while exploring innovative methods currently available for remote sensing of vegetation monitoring. Therefore, the imagery was acquired and pre-processed without ground control points so as to minimize flight planning costs and user interaction, while the classification was based exclusively on the spectral and altitudinal information derived from the imagery using 3D photo-reconstruction methods.

Results obtained demonstrate the effectiveness of this kind of technology even in high complex agricultural areas, both regarding the digital surface model reconstruction and the subsequent terrace classification stage. We obtained an average RMSE lower than 0.5 m in the DSM local elevation gradients and an overall classification accuracy of 90% using an object-oriented approach. In this approach, altitudinal and spectral information was analyzed at different scales taking into account the spatial context and morphology of the objects on the image. Therefore, this methodology can be used for the implementation and monitoring of CAP measures. Indeed, its application to time series of images makes it possible to monitor the persistence of agricultural terraces as ecosystem service providers. This method can also be extended for the identification and monitoring of other elements such as landscape features (e.g. isolated trees, tree lines, hedgerows) on agricultural land, as an interesting topic for further research.

Use of very high resolution UAV imagery has advantages compared to traditional photogrammetric or satellite remote sensing data. Most of these advantages are related to its fast on-the-spot data acquisition and simple processing requirements. This makes it particularly advisable for quick and cost effective verification in areas comprising several hundred of hectares.

## Acknowledgments

We would like to thank S. Calvo and D. Fasbender for their constructive comments on data analysis. A. Gomez, D. Notario, A. Vera, A. Hornero and R. Romero (QuantaLab-IAS-CSIC research laboratory, Spain) are acknowledged for their contribution during the airborne and field campaigns.

## Appendix A. Supplementary data

Supplementary data related to this article can be found at <http://dx.doi.org/10.1016/j.jenvman.2014.01.006>.

## References

- Agnoletti, M., Cargnello, G., Gardin, L., Santoro, A., Bazzoffi, P., Sansone, L., Pezza, L., Belfiore, N., 2011. Traditional landscape and rural development: comparative study in three terraced areas in northern, central and southern Italy to evaluate the efficacy of GAEC standard 4.4 of cross compliance. *Italian J. Agron.* 6, 121–139.
- Aksoy, S., Akçay, H.G., Wassenaar, T., 2010. Automatic mapping of linear woody vegetation features in agricultural landscapes using very high resolution imagery. *IEEE Transact. Geosci. Remote Sens.* 48, 511–522.
- Amorós López, J., Izquierdo Verdiguier, E., Gómez Chova, L., Muñoz Marí, J., Rodríguez Barreiro, J.Z., Camps Valls, G., Calpe Maravilla, J., 2011. Land cover classification of VHR airborne images for citrus grove identification. *ISPRS J. Photogr. Remote Sens.* 66, 115–123.
- Artuso, R., Bovet, S., Streilein, A., 2003. Practical methods for the verification of countrywide produced terrain and surface models. In: Maas, H.-G., Vosselman, G. (Eds.), *ISPRS Archives – Volume XXXIV-3/W13, 2003. WG III/3. 3-D Reconstruction from Airborne Laserscanner and InSAR Data*, p. 6. Dresden, Germany.
- Åstrand, P.J., Bongiorno, M., Crespi, M., Fratarcangeli, F., Da Costa, J.N., Peralice, F., Walczynska, A., 2012. The potential of WorldView-2 for ortho-image production within the "Control with Remote Sensing Programme" of the European Commission. *Int. J. Appl. Earth Observ. Geoinf.* 19, 335–347.
- Baatz, M., Benz, U., Dehghani, S., Heynen, M., Höltje, A., Hofmann, P., Lingensfelder, I., Mimler, M., Sohlbach, M., Weber, M., Willhauck, G., 2004. *ECognition Professional User Manual 4*. Definiens Imaging, München.
- Bailly, J.-S., Levassieur, F., 2012. Potential of linear features detection in a Mediterranean landscape from 3D VHR optical data: application to terrace walls. In: *Geoscience and Remote Sensing Symposium (IGARSS), 2012 IEEE International*. Benz, U.C., Hofmann, P., Willhauck, G., Lingensfelder, I., Heynen, M., 2004. Multi-resolution, object-oriented fuzzy analysis of remote sensing data for GIS-ready information. *ISPRS J. Photogr. Remote Sens.* 58, 239–258.
- Berni, J.A.J., Zarco-Tejada, P.J., Suarez, L., Fereres, E., 2009a. Thermal and narrow-band multispectral remote sensing for vegetation monitoring from an unmanned aerial vehicle. *IEEE Transact. Geosci. Remote Sens.* 47 (3), 722–738.
- Berni, J.A.J., Zarco-Tejada, P.J., Sepulcre-Cantó, G., Fereres, E., Villalobos, F.J., 2009b. Mapping canopy conductance and CWSI in olive orchards using high resolution thermal remote sensing imagery. *Remote Sens. Environ.* 113, 2380–2388.
- Bishop, Y.M.M., Fienberg, S.E., Holland, P.W., 1975. *Discrete Multivariate Analysis: Theory and Practice*. MIT Press, Cambridge, Massachusetts, p. 36. European Commission, 2004. *The Common Agricultural Policy explained*. Directorate General Agriculture and Rural Development. Publications Office of the European Union.
- Blaschke, T., 2010. Object based image analysis for remote sensing. *ISPRS J. Photogr. Remote Sens.* 65, 2–16.
- Burnett, C., Blaschke, T., 2003. A multi-scale segmentation/object relationship modelling methodology for landscape analysis. *Ecol. Model.* 168, 233–249.
- Capaldo, P., Crespi, M., De Vendictis, L., Fratarcangeli, F., Murchio, G., Nascetti, A., Peralice, F., 2010. Geometric potentiality of GeoEye-1 in-track stereo pairs and accuracy assessment of generated digital surface models. In: Reuter, R. (Ed.), *30th Annual EARSeL Symposium. Remote Sensing for Science, Education, and Natural and Cultural Heritage*. Paris, pp. 483–490.
- Castilla, G., Hay, G.J., 2008. Image objects and geographic objects. In: Blaschke, T.L., Stefan, Hay, G. (Eds.), *Object-based Image Analysis: Spatial Concepts for Knowledge-driven Remote Sensing Applications, Lecture Notes in Geo-information and Cartography*. Springer-Verlag, Berlin, pp. 91–110.

- Clarke, J.D.A., Gibson, D., Apps, H., 2010. The use of LiDAR in applied interpretive landform mapping for natural resource management, Murray River alluvial plain, Australia. *Int. J. Remote Sens.* 31, 6275–6296.
- Congalton, R.G., 1991. A review of assessing the accuracy of classifications of remotely sensed data. *Remote Sens. Environ.* 37, 35–46.
- Congalton, R., Green, K., 1999. *Assessing the Accuracy of Remotely Sensed Data: Principles and Practices*. Lewis Publishers., Boca Raton, Florida.
- Demoulin, A., Bovy, B., Rixhon, G., Cornet, Y., 2007. An automated method to extract fluvial terraces from digital elevation models: the Vesdre valley, a case study in eastern Belgium. *Geomorphology* 91, 51–64.
- Drăguț, L., Blaschke, T., 2006. Automated classification of landform elements using object-based image analysis. *Geomorphology* 81, 330–344.
- Drăguț, L., Tiede, D., Levick, S.R., 2010. ESP: a tool to estimate scale parameter for multiresolution image segmentation of remotely sensed data. *Int. J. Geogr. Inf. Sci.* 24, 859–871.
- Dunjó, G., Pardini, G., Gispert, M., 2003. Land use change effects on abandoned terraced soils in a Mediterranean catchment, NE Spain. *CATENA* 52, 23–37.
- European Commission, 2012a. *The Common Agricultural Policy a Partnership between Europe and Farmers*. Directorate General Agriculture and Rural Development. Publications Office of the European Union, p. 16.
- European Commission, 2012b. *Guidelines for Best Practice and Quality Checking of Ortho Imagery*. Available at: <http://marswiki.jrc.ec.europa.eu/wikicap/index.php/> (Last access 20/03/2012).
- Faulkner, H., Ruiz, J., Zukowskyj, P., Downward, S., 2003. Erosion risk associated with rapid and extensive agricultural clearances on dispersive materials in southeast Spain. *Environ. Sci. Policy* 6, 115–127.
- Fielding, A.H., Bell, J.F., 1997. A review of methods for the assessment of prediction errors in conservation presence/absence models. *Environ. Conserv.* 24, 38–49.
- Fleiss, J.L., 1981. *Statistical Methods for Rates and Proportions*, second ed. John Wiley, New York.
- Foody, G.M., 2002. Status of land cover classification accuracy assessment. *Remote Sens. Environ.* 80, 185–201.
- González-Dugo, V., Zarco-Tejada, P.J., Berni, J.A., Suarez, L., Goldhamer, D., Fereres, E., 2012. Almond tree canopy temperature reveals intra-crown variability that is water stress-dependent. *Agric. For. Meteorol.* 154–155, 156–165.
- Guillén-Climent, M.L., Zarco-Tejada, P.J., Berni, J.A.J., North, P.R.J., Villalobos, F.J., 2012. Mapping radiation interception in row-structured orchards using 3D simulation and high resolution airborne imagery acquired from a UAV. *Precis. Agric.* 13, 473–500.
- Hou, W., Walz, 2013. Enhanced analysis of landscape structure: inclusion of transition zones and small-scale landscape elements. *Ecol. Indic.* 31, 15–24.
- Hofmann, P., Blaschke, T., Strobl, J., 2011. Quantifying the robustness of fuzzy rule sets in object-based image analysis. *Int. J. Remote Sens.* 32, 7359–7381.
- James, M.R., Robson, S., 2012. Straightforward reconstruction of 3D surfaces and topography with a camera: accuracy and geoscience application. *J. Geophys. Res. Earth Surf.* 117, F03017.
- Karydas, C.G., Sekulowska, T., Sarakiotis, I., 2005. Fine scale mapping of agricultural landscape features to be used in environmental risk assessment in an olive cultivation area. *IASME Trans.* 4, 582–589.
- Krauß, T., Arefi, H., Reinartz, P., 2011. Evaluation of selected methods for extracting digital terrain models from satellite born digital surface models in urban areas. In: *SMPR2011*. Tehran, Iran.
- Küng, O., Strelcha, C., Beyeler, A., Zufferey, J.-C., Floreano, D., Fua, P., Gervais, F., 2011. The accuracy of automatic photogrammetric techniques on ultra-light UAV imagery. *ISPRS - Int. Arch. Photogr., Remote Sens. Spatial Inf. Sci.* XXXVIII-1, 125–130.
- Laliberte, A.S., Browning, D.M., Herrick, J.E., Gronemeyer, P., 2010. Hierarchical object-based classification of ultra-high-resolution digital mapping camera (DMC) imagery for rangeland mapping and assessment. *J. Spatial Sci.* 55, 101–115.
- Landis, J.R., Koch, G.G., 1977. The measurement of observer agreement for categorical data. *Biometrics* 33, 159–174.
- Li, Y., Gong, J., Wang, D., An, L., Li, R., 2012. Sloping farmland identification using hierarchical classification in the Xi-He region of China. *Int. J. Remote Sens.* 34, 545–562.
- Martínez-Casasnovas, J.A., Ramos, M.C., Cots-Folch, R., 2010. Influence of the EU CAP on terrain morphology and vineyard cultivation in the Priorat region of NE Spain. *Land Use Policy* 27, 11–21.
- McNab, W.H., 1989. Terrain shape index: quantifying effect of minor landforms on tree height. *For. Sci.* 35, 91–104.
- McNeill, J.R., 1992. *The Mountains of the Mediterranean World: an Environmental History*. Cambridge University Press, Cambridge.
- Pereira, H.M., Domingos, T., Vicente, L., 2006. Assessing ecosystem services at different scales in the Portugal Millennium Ecosystem Assessment. In: Reid, W.V., Berkes, F., Wilbanks, T., Capistrano, D. (Eds.), *Millennium Ecosystem Assessment, Bridging Scales and Epistemologies*. Island Press, Washington, pp. 59–79.
- Reid, A., Ramos, F., Sukkarieh, S., 2011. Multi-class classification of vegetation in natural environments using an unmanned aerial system. In: *Proceedings - IEEE International Conference on Robotics and Automation*. Australian Centre for Field Robotics, University of Sydney, NSW, 2006, Australia, pp. 2953–2959.
- Rey Benayas, J.M., Martins, A., Nicolau, J.M., Schulz, J.J., 2007. Abandonment of agricultural land: an overview of drivers and consequences. *Cab. Rev. Perspect. Agric. Veterinary Sci. Nutr. Nat. Resour.* 2 (057), 14.
- Sheeren, D., Bastin, N., Ouin, A., Ladet, S., Balent, G., Lacombe, J.P., 2009. Discriminating small wooded elements in rural landscape from aerial photography: a hybrid pixel/object-based analysis approach. *Int. J. Remote Sens.* 30, 4979–4990.
- Suárez, L., Zarco-Tejada, P.J., González-Dugo, V., Berni, J.A.J., Sagardoy, R., Morales, F., Fereres, E., 2010. Detecting water stress effects on fruit quality in orchards with time-series PRI airborne imagery. *Remote Sens. Environ.* 114, 286–298.
- Tagil, S., Jenness, J., 2008. GIS-based automated landform classification and topographic, land cover and geologic attributes of landforms around the Yazoren Polje, Turkey. *J. Appl. Sci.* 8, 910–921.
- Tansey, K., Chambers, I., Anstee, A., Denniss, A., Lamb, A., 2009. Object-oriented classification of very high resolution airborne imagery for the extraction of hedgerows and field margin cover in agricultural areas. *Appl. Geogr.* 29, 145–157.
- Tortora, R., 1978. A note on sample size estimation for multinomial populations. *Am. Stat.* 32, 100–102.
- Wallace, L., Lucieer, A., Watson, C., Turner, D., 2012. Development of a UAV-LiDAR system with application to forest inventory. *Remote Sens.* 4, 1519–1543.
- Waser, L.T., Baltasvias, E., Ecker, K., Eisenbeiss, H., Feldmeyer-Christe, E., Ginzler, C., Küchler, M., Zhang, L., 2008. Assessing changes of forest area and shrub encroachment in a mire ecosystem using digital surface models and CIR aerial images. *Remote Sens. Environ.* 112, 1956–1968.
- Zaman, B., Jensen, A.M., McKee, M., 2011. Use of high-resolution multispectral imagery acquired with an autonomous unmanned aerial vehicle to quantify the spread of an invasive wetlands species. In: *International Geoscience and Remote Sensing Symposium (IGARSS)*. Utah Water Research Laboratory, Utah State University, 8200 Old Main Hill, Logan, UT 84322-8200, United States, pp. 803–806.
- Zarco-Tejada, P.J., Berni, J.A.J., Suárez, L., Fereres, E., 2008. A new era in remote sensing of crops with unmanned robots. *SPIE Newsroom*. <http://dx.doi.org/10.1117/2.1200812.143>.
- Zarco-Tejada, P.J., Berni, J.A.J., Suárez, L., Sepulcre-Cantó, G., Morales, F., Miller, J.R., 2009. Imaging chlorophyll fluorescence from an airborne narrow-band multi-spectral camera for vegetation stress detection. *Remote Sens. Environ.* 113, 1262–1275.
- Zarco-Tejada, P.J., González-Dugo, V., Berni, J.A.J., 2012. Fluorescence, temperature and narrow-band indices acquired from a UAV platform for water stress detection using a micro-hyperspectral imager and a thermal camera. *Remote Sens. Environ.* 117, 322–337.
- Zarco-Tejada, P.J., Morales, A., Testi, L., Villalobos, F.J., 2013a. Spatio-temporal patterns of chlorophyll fluorescence and physiological and structural indices acquired from hyperspectral imagery as compared with carbon fluxes measured with eddy covariance. *Remote Sens. Environ.* 133, 102–115.
- Zarco-Tejada, P.J., Guillén-Climent, M.L., Hernández-Clemente, R., Catalina, A., González, M.R., Martín, P., 2013b. Estimating leaf carotenoid content in vineyards using high resolution hyperspectral imagery acquired from an unmanned aerial vehicle. *Agric. For. Meteorol.* 171–172, 281–294.